DOI: 10.1002/ejic.200800309

Adipato-Bridged Copper(II) Complexes

Yue-Qing Zheng,*[a] De-Yi Cheng,[a] Jian-Li Lin,[a] Zhi-Feng Li,[a] and Xian-Wen Wang[a]

Keywords: Copper / Cluster compounds / Bridging ligands / Carboxylate ligands / Coordination polymers

Reactions of $Cu(ClO_4)_2·6H_2O$, adipic acid, and 2,2′-bipyridine/1,10-phenanthroline in aqueous methanolic solutions afforded four adipato-bridged Cu^{II} complexes, $\{[Cu(phen)_2]_2(C_6H_8O_4)\}(ClO_4)_2$ (**1**), $\{[Cu(phen)_2]_2(C_6H_8O_4)\}(ClO_4)_2·1.33H_2O$ (**2**), $[Cu_2(phen)_2(H_2O)]_2(C_6H_8O_4)_2(ClO_4)_4$ (**3**), and $\{[Cu_2(bpy)_2(H_2O)]_2(C_6H_8O_4)_2\}(ClO_4)_4·2H_2O$ (**4**) (phen = 1,10-phenanthroline, bpy = 2,2′-bipyridine, $C_6H_8O_4$ = adipate anion). The centrosymmetric adipato-bridged dumbbell-like dinuclear complex cations $\{[Cu(phen)_2]_2(C_6H_8O_4)\}^{2+}$ in **1** and **2**, through aromatic stacking interactions, are assembled into supramolecular (4,4) networks, and twofold interpenetration of the networks completes the 3D supramolecular architectures with counterions as well as the lattice water molecules in voids. The characteristic secondary building units in **3** and **4** are the centrosymmetric double-semi-paddle-wheel of tetranuclear $\{[Cu_2(phen)_2(H_2O)]_2(COO)_4\}$ and$\{[Cu_2(bpy)_2(H_2O)]_2(COO)_4\}$ clusters, respectively, which are interconnected by adipato ligands to form (4,4) networks. The resulting networks, through interlayer-stacking interactions, are assembled into a 3D open framework with counterions as well as the lattice water molecules in channels. Magnetic studies of **3** and **4** suggest significant antiferromagnetic coupling interactions between Cu^{II} ions bridged by the *syn–syn* carboxylate groups, whereas weak ferromagnetic coupling is observed between two symmetry-related copper(II) ions bridged by the μ_2-O atoms. Cyclic voltammograms of **3** and **4** exhibit similar redox behaviors and display two quasi-reversible couples. The thermal decompositions of **3** and **4** are also described.

Introduction

Because of their intriguing architectures and properties for potential applications in the fields of catalysis, host–guest chemistry, magnetic materials, and photoelectrical materials, supramolecular complexes and coordination polymers have attracted much attention.[1–3] For assembly of supramolecular systems and construction of coordination polymers, polynuclear metal clusters have been widely used as secondary building units (SBUs). Among them, polynuclear copper clusters are of especial interest due to their attracting structures as well as their potential applications in molecule-based magnet, multielectron redox processes, and catalysis.[4–6] In past decades, a variety of oligocopper clusters derived from Cu^{II} and carboxylate anions have been studied.[7–9] A notable class of these is paddle-wheel-like tetracarboxylate dicopper clusters $[Cu_2(COO)_4]$, where two copper ions are bridged by four carboxylate groups in the *syn–syn* mode.[10–12] The tetracarboxylato-bridged dicopper clusters have been found to be good candidates for SBUs in the construction of rigid open metal-organic frameworks (MOFs).[13–15] For example, Zaworotko et al. reported several examples of coordination polymers with the tetracarboxylato-bridged dimetallic clusters as SBUs by using 1,3-benzene-dicarboxylic acid and glutaric acid, respectively, as organic linkers.[16,17]

Interestingly, research has indicated that carboxylate groups in the above-mentioned paddle-wheel-like tetracarboxylato-bridged copper(II) dimers could be pairwise replaced by bidentate N-donor aromatic ligands to form semi-paddle-wheel (SPW) dinuclear clusters,[18–19] which, through two *anti–syn* bridging carboxylate oxygen atoms, could be further condensed into double-semi-paddle-wheel (DSPW) tetranuclear copper(II) clusters (Scheme 1).[20–21] Such DSPW-like tetranuclear copper(II) clusters have been found in molecular complexes;[20–21] however, it is seldom that they have been used as SBUs to construct coordination polymers. Our recent investigations show that self-assembly of Cu^{II} ions and adipate anions in the presence of 2,2-bipyridine (bpy) or 1,10-phenanthroline (phen) provides an efficient strategy for nucleation of DSPW-like tetranuclear copper(II) clusters, which can be bridged by adipato ligands to make up porous MOFs. The present contribution reports the results of four adipato-bridged Cu^{II} bpy/phen complexes $\{[Cu(phen)_2]_2(C_6H_8O_4)\}·(ClO_4)_2$ (**1**), $\{[Cu(phen)_2]_2(C_6H_8O_4)\}(ClO_4)_2·1.33H_2O$(**2**),$[Cu_2(phen)_2(H_2O)]_2(C_6H_8O_4)_2(ClO_4)_4$ (**3**), and $\{[Cu_2(bpy)_2(H_2O)]_2(C_6H_8O_4)_2\}(ClO_4)_4·2H_2O$ (**4**). Complexes **1** and **2** display 3D supramolecular architectures with (4,4) interpenetrating topologies, whereas

[a] Institute of Solid Materials Chemistry,
State Key Laboratory Base of Novel Functional Materials & Preparation Science,
Faculty of Materials Science & Chemical Engineering,
Ningbo University, Ningbo 315211, P. R. China
Fax: +86-574-87600747
E-mail: zhengcm@nbu.edu.cn

Supporting information for this article is available on the WWW under http://www.eurjic.org or from the author.

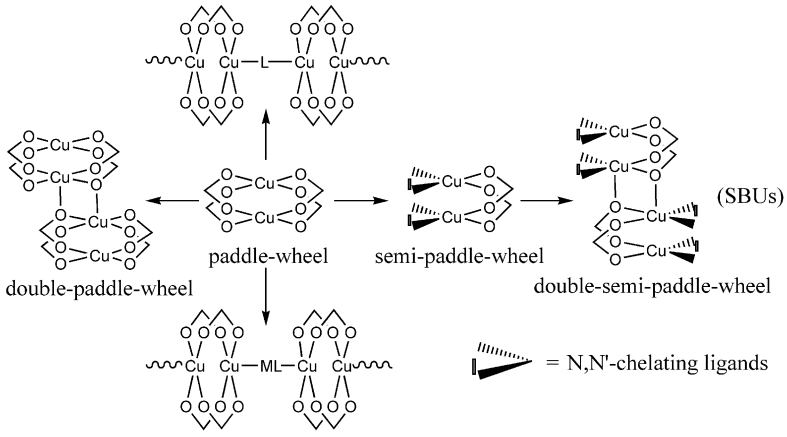

Scheme 1.

complexes **3** and **4** feature 2D porous polymeric networks generated form DSPW-like tetranuclear copper(II) clusters bridged by adipato ligands.

Results and Discussion

Syntheses

Reactions of equivalent molar ratios of $Cu(ClO_4)_2 \cdot 6H_2O$, adipic acid, and 2,2′-bipyridine/1,10-phenanthroline can only afford the reported complexes, $[Cu(bpy)_2(ClO_4)](ClO_4)$ and $[Cu(phen)_2(H_2O)](ClO_4)_2$.[22,23] When the reaction system was neutralized to 7.0, a mixture of **1** and **2** was obtained in presence of phenanthroline and **4** was isolated in presence of 2,2′-bipyridine. The molar ratio of $Cu(ClO_4)_2 \cdot 6H_2O$, adipic acid, and 1,10-phenanthroline was tuned to 1:0.5:1 and the pH value adjusted to 7, resulting in **3** by slow evaporation of the suspension. The blue deposition was considered to determine the material ratio in the supernatant and facilitate the crystal growth of **3**.

Structure Descriptions

Compound 1

Compound **1** consists of dinuclear Cu^{II} complex cations $\{[Cu(phen)_2]_2(C_6H_8O_4)\}^{2+}$ and perchlorate anions. As shown in Figure 1a, The complex cation displays a centrosymmetric dumbbell structure, in which two $[Cu(phen)_2]$ moieties are bridged by an adipate ligand with the Cu···Cu separation of 11.849(3) Å. Each Cu^{II} ion is located in a square-pyramidal geometry defined by four N atoms of two chelating phen ligands and one O atom of an adipato ligand with an N atom at the apex. The τ (Addison) value of 0.07 (τ = 0 for an ideal square pyramid and τ = 1 for an ideal trigonal bipyramid)[24] indicates no significant distortion of the geometry. The bond lengths of Cu–O and Cu–N in **1** are 1.964(5) and 2.007–2.209 Å, respectively, comparable with those in the known copper(II) adipate complexes, $[Cu(phen)_2(C_6H_8O_4)] \cdot 4.5H_2O$ and $[(Cu_2(phen)_2Cl_2)(C_6H_8O_4)] \cdot 4H_2O$.[25] The two terminal phen rings at each Cu^{II} ion orientate nearly perpendicularly to each other with a dihedral angle of 79.0°, and the phen ligands are found to be engaged in intercationic face-to-face π–π stacking interactions (mean interplanar distance: 3.37 Å). The uncoordinated O atoms of the adipate ligand are involved in weak intercationic C–H···O hydrogen bonds with the neighboring phen ligands (3.073 Å). As depicted in Figure 1b, the intercationic π–π stacking as well as C–H···O hydrogen bonding interactions are responsible for assembly of the complex cations into 2D supramolecular (4,4) networks parallel to (110) and (1$\bar{1}$0), respectively. They interpenetrate each other

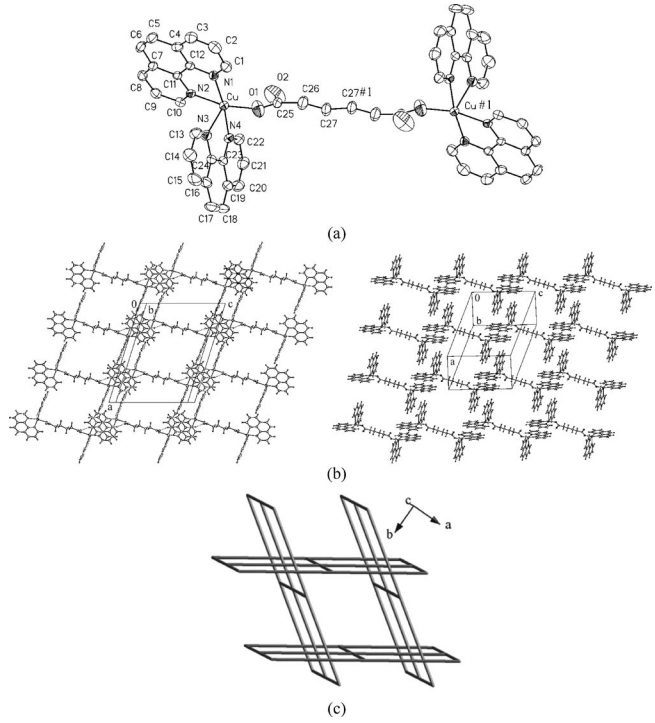

Figure 1. (a) ORTEP view of the complex cations in **1** together with atom numbering scheme and thermal ellipsoids drawn at 30% probability level (symmetry codes: #1 = –*x* + 1/2, –*y* + 1/2, –*z* + 1); (b) assembly of complex cations into (4,4) supramolecular networks; (c) a twofold interpenetration topology of the (4,4) supramolecular networks.

Table 1. Selected bond lengths (Å) and angles (°) of **1** and **2**.

1		**2**					
Cu1–O1	1.964(5)	Cu1–O4	1.982(4)	O4–Cu1–N5	88.9(2)	N9–Cu2–N11	92.5(1)
Cu1–N1	2.007(4)	Cu1–N5	2.216(3)	O4–Cu1–N6	93.6(1)	N9–Cu2–N12	173.4(2)
Cu1–N2	2.066(4)	Cu1–N6	1.999(4)	O4–Cu1–N7	92.3(2)	N10–Cu2–N11	102.4(1)
Cu1–N3	2.209(4)	Cu1–N7	2.001(4)	O4–Cu1–N8	163.2(2)	N10–Cu2–N12	99.2(1)
Cu1–N4	2.016(4)	Cu1–N8	2.061(3)	N5–Cu1–N6	79.1(1)	N11–Cu2–N12	81.7(1)
O1–Cu1–N1	91.6(2)	Cu2–O6	1.955(4)	N5–Cu1–N7	96.9(1)	O2–Cu3–N1	89.9(2)
O1–Cu1–N2	167.1(2)	Cu2–N9	1.991(3)	N5–Cu1–N8	107.2(1)	O2–Cu3–N2	163.2(2)
O1–Cu1–N3	91.8(2)	Cu2–N10	2.250(4)	N6–Cu1–N7	172.8(2)	O2–Cu3–N3	90.6(2)
O1–Cu1–N4	93.6(2)	Cu2–N11	2.045(3)	N6–Cu1–N8	94.1(1)	O2–Cu3–N4	95.9(1)
N1–Cu1–N2	81.3(2)	Cu2–N12	2.008(3)	N7–Cu1–N8	81.3(1)	N1–Cu3–N2	81.1(2)
N1–Cu1–N3	93.5(2)	Cu3–O2	1.938(4)	O6–Cu2–N9	94.3(1)	N1–Cu3–N3	99.2(1)
N1–Cu1–N4	171.4(2)	Cu3–N1	2.008(4)	O6–Cu2–N10	91.5(2)	N1–Cu3–N4	173.7(2)
N2–Cu1–N3	99.3(2)	Cu3–N2	2.043(4)	O6–Cu2–N11	165.4(2)	N2–Cu3–N3	104.8(1)
N2–Cu1–N4	94.8(2)	Cu3–N3	2.225(4)	O6–Cu2–N12	92.1(2)	N2–Cu3–N4	93.8(1)
N3–Cu1–N4	79.5(2)	Cu3–N4	2.020(4)	N9–Cu2–N10	78.9(1)	N3–Cu3–N4	78.4(1)

to generate 3D supramolecular architectures (Figure 1c). The disordered ClO_4^- anions fill in the interspace and are hydrogen bonded to phenanthroline. Obviously, they make an additional contribution to the stabilization of the crystal structure. Selected bond lengths and angles for **1** are listed in Table 1.

Compound 2[26]

Similar to **1**, the principal building units in compound **2** are also the dinuclear Cu^{II} complex cations (Figure 2a). The asymmetric unit of **2** is composed of three Cu^{II} ions, six phen ligands, one and a half adipate ligands, three perchlorate counter anions, and two lattice water molecules. The Cu^{II} ions are all disposed in a N_4O square-pyramidal coordination environment with the Cu–O bond lengths ranging from 1.938 to 1.983 Å and equatorial and apical Cu–N bond lengths in the regions 1.991–2.060 and 2.217–2.250 Å, respectively. The separation of Cu1···Cu2 and Cu3···Cu3$^{\#1}$ are 11.33(8) and 11.7(1) Å shorter than the distance in **1**. The τ (Addison) parameters of 0.12, 0.17, and 0.18 for Cu1, Cu2, and Cu3, respectively, indicate slightly larger distortions of the square-pyramidal coordination in **2** than in **1**. Due to the intercationic π–π stacking as well as C–H···O hydrogen bonding interactions, the complex cations are assembled into 2D supramolecular (4,4) networks parallel to (010) and (11$\bar{1}$), respectively, as illustrated in Figure 2b. Just as **1**, the resulting (4,4) networks are interpenetrated with each other to form open 3D supramolecular architecture with the perchlorate anions and the lattice water molecules located in voids and engaged in hydrogen bonds to the adjacent phenanthroline ligands. According to the above structure descriptions, compound **2** is practically a hydrated one of **1**. Selected bond lengths and angles for **2** are listed in Table 1.

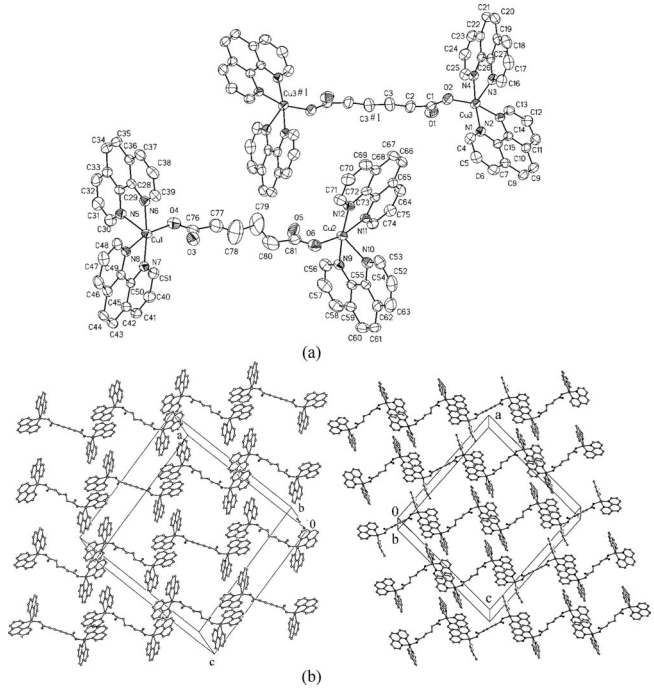

Figure 2. (a) ORTEP view of the complex cations in **2** together with atom numbering scheme and thermal ellipsoids drawn at 30% probability level (symmetry codes: #1 = –*x* + 2, –*y* + 1, –*z*); (b) assembly of complex cations into (4,4) supramolecular networks.

Compound 3

This compound consists of perchlorate anions and positively charged 2D layers $\{[Cu_2(phen)_2(H_2O)]_2(C_6H_8O_4)_2\}_n$ characteristic of (4,4) topology. As illustrated in Figure 3a, the SBUs are centrosymmetric DSPW tetranuclear copper(II) clusters $\{[Cu_2(phen)_2(H_2O)]_2(COO)_4\}$, which result from condensation of two SPW-like dinuclear copper units through two *anti–syn* bridging carboxylate oxygen atoms. The separation of Cu1···Cu2 and Cu2···Cu2$^{\#1}$ (#1 = –*x* + 1, –*y*, –*z* + 1) within the tetranuclear cluster are 2.9565(9) and 3.356(1) Å, respectively. As stated above (Scheme 1), the SPW units originate from replacement of two carboxylate groups in the classic $[Cu_2(COO)_4]$ clusters by two phen ligands. Both crystallographically independent Cu1 and Cu2 atoms are located in the similar CuN_2O_3 square-pyramidal coordination environment with the basal plane defined by two N atoms of the phen ligand and two O atoms

of two adipate ligands and the apical sites occupied by an aqua oxygen atom and an *anti–syn* bridging carboxylate oxygen atom for Cu1 and Cu2, respectively. The equatorial Cu–O and Cu–N bond lengths fall in the range 1.921(3)–1.964(2) and 1.998(3)–2.004(3) Å, respectively, and the axial Cu–O bond length of 2.205(3) Å to the aqua oxygen atom is significantly shorter than that of 2.432(3) Å to the *anti–syn* bridging carboxylate oxygen atom due to steric effects. The bond length and angle parameters suggest slight distortions of the square-pyramidal coordination sphere with 0.12 Å (Cu1) and 0.08 Å (Cu2). The two crystallographically distinct adipate anions are each imposed by a symmetry inversion center and exhibit two different bridging modes: one acting as bis(bidentate) ligand bridging four Cu atoms and the other bridging six Cu atoms with one carboxylate oxygen atom in an *anti–syn* bridging fashion. The centrosymmetric $\{[Cu_2(phen)_2(H_2O)]_2(COO)_4\}$ DSPWs function as 4-connected SBUs and the phenanthroline rings coordinating Cu1 and Cu2, respectively, exhibit nearly perfect coplanarity and orientate nearly parallelly to each other with a dihedral angle of 5.4° and the mean interplanar distance of 3.37 Å suggests significant intracluster-stacking interactions. The four-connected DSPWs are interlinked by adipato-bridging ligands to form 2D (4,4) layers parallel to (100), and the resulting layers are stacked in such a way that the phenanthroline ligands are engaged in the interlayer-stacking interactions (mean interplanar distance: 3.41 Å) to form 1D rhombic channels propagating along the [100] direction with the perchlorate anions located in the channels (Figure 3b). The perchlorate anions are hydrogen bonded to the water molecules with O–H···O bonds (2.882–3.112 Å) as well as to the phenanthroline ligands with C–H···O bonds (3.190–3.325 Å). Selected bond lengths and angles for **3** are listed in Table 2.

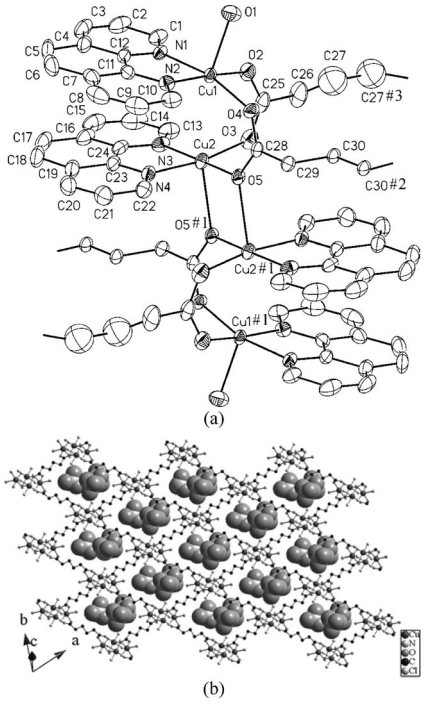

Figure 3. ORTEP view of the DSPW-like tetranuclear copper(II) clusters in **3** with atom numbering scheme and thermal ellipsoids drawn at 30% probability level (symmetry codes: #1 = $-x + 1$, $-y$, $-z + 1$; #2 = $-x$, $-y$, $-z + 1$; #3 = $-x$, $-y + 1$, $-z + 1$); (b) crystal structure of **3** with perchlorate anions in space-filling mode (note that the coordinated phenanthroline rings were omitted for clarity except the nitrogen atoms).

Compound 4

This compound features (4,4) 2D cationic layers $\{[Cu_2(bpy)_2(H_2O)]_2(C_6H_8O_4)_2\}_n$ exhibiting an extremely similar structure to that of **3** with 2,2-bipyridine instead of phenanthroline.[27] The separation of Cu1···Cu2 and Cu2···Cu2$^{\#1}$ (#1 = $-x + 1$, $-y + 1$, $-z$) within the DSPW unit are 2.973(1) and 3.378(1) Å, respectively, longer than the corresponding distances in **3**. The centrosymmetric

Table 2. Selected bond lengths (Å) and angles (°) of **3** and **4**.

3							
Cu1–O1	2.204(3)	Cu1–N1	2.004(3)	Cu2–O5	1.964(2)	Cu2–N3	1.998(3)
Cu1–O2	1.938(3)	Cu1–N2	1.998(3)	Cu2–O5$^{\#1}$	2.432(3)	Cu2–N4	2.004(3)
Cu1–O4	1.958(2)	Cu2–O3	1.921(3)				
O1–Cu1–O2	92.1(1)	O2–Cu1–N1	93.8(1)	O3–Cu2–O5	90.8(1)	O5–Cu2–N3	175.5(1)
O1–Cu1–O4	97.7(1)	O2–Cu1–N2	173.0(1)	O3–Cu2–O5$^{\#1}$	97.6(1)	O5–Cu2–N4	93.1(1)
O1–Cu1–N1	95.3(1)	O4–Cu1–N1	166.0(1)	O3–Cu2–N3	93.1(1)	O5$^{\#1}$–Cu2–N3	100.8(1)
O1–Cu1–N2	94.0(1)	O4–Cu1–N2	91.7(1)	O3–Cu2–N4	170.5(1)	O5$^{\#1}$–Cu2–N4	91.6(1)
O2–Cu1–O4	90.8(1)	N1–Cu1–N2	82.3(1)	O5–Cu2–O5$^{\#1}$	81.0(9)	N3–Cu2–N4	82.7(1)
Symmetry codes: #1 = $-x + 1$, $-y$, $-z + 1$							
4							
Cu1–O1	2.214(4)	Cu1–N1	1.989(3)	Cu2–O5	1.962(3)	Cu2–N3	1.982(3)
Cu1–O2	1.951(3)	Cu1–N2	1.992(3)	Cu2–O5$^{\#1}$	2.498(3)	Cu2–N4	1.980(3)
Cu1–O4	1.959(3)	Cu2–O3	1.931(3)				
O1–Cu1–O2	88.5(1)	O2–Cu1–N1	175.8(1)	O3–Cu2–O5	88.9(1)	O5–Cu2–N3	94.8(1)
O1–Cu1–O4	101.6(1)	O2–Cu1–N2	94.9(1)	O3–Cu2–O5$^{\#1}$	96.8(1)	O5–Cu2–N4	177.0(1)
O1–Cu1–N1	93.8(2)	O4–Cu1–N1	93.2(1)	O3–Cu2–N3	169.2(1)	O5$^{\#2}$–Cu2–N3	93.7(1)
O1–Cu1–N2	94.3(2)	O4–Cu1–N2	163.5(1)	O3–Cu2–N4	94.1(1)	O5$^{\#2}$–Cu2–N4	97.0(1)
O2–Cu1–O4	89.9(1)	N1–Cu1–N2	81.4(1)	O5–Cu2–O5$^{\#1}$	82.3(1)	N3–Cu2–N4	82.3(1)
Symmetry codes: #1 = $-x + 1$, $-y + 1$, $-z$							

{[$Cu_2(bpy)_2(H_2O)$]$_2$($COO)_4$} DSPWs (Figure 4a) are stabilized by significant intracluster-stacking interactions between bpy ligands and are interconnected by adipato ligands into polymeric networks. The formed layers are further, through interlayer-stacking interactions between adjacent bpy ligands, assembled into 3D supramolecular framework with rhombic channels filled with the hydrogen-bonded perchlorate anions and lattice water molecules (Figure 4b). Similar to **3**, the Cu atoms in **4** are each square pyramidally coordinated by two nitrogen atoms from one bpy ligand and three oxygen atoms from two carboxylate groups and one aqua ligand from three carboxylate groups to complete the CuN_2O_3 chromophores. The apical ligating atoms are an aqua oxygen atom and an *anti–syn* bridging carboxylate oxygen atom, respectively, at Cu1 and Cu2. The equatorial Cu–N bond lengths in the range 1.980(3)–1.992(3) Å are shorter than those in **3**, but they are comparable with the corresponding ones in [Cu_{12}(tidhd)$_4$(CH_3OH)$_8$($CH_3COO)_8$]($CH_3OH)_{0.8}$ [Htidhd = 1,1,7,7-tetrakis(imidazol-2-yl)-2,6-diaza-1,6-heptadiene],[21] whereas the basal and apical Cu–O bond lengths vary in the ranges 1.931–1.962 and 2.214–2.498(3) Å, respectively, and are longer than the corresponding ones in **3**. The τ (Addison) parameters of 0.20 (Cu1) and 0.13 (Cu2) indicate more significant distortion of the square-pyramidal coordination geometry around Cu atoms. Selected bond lengths and angles for **4** are listed in Table 2.

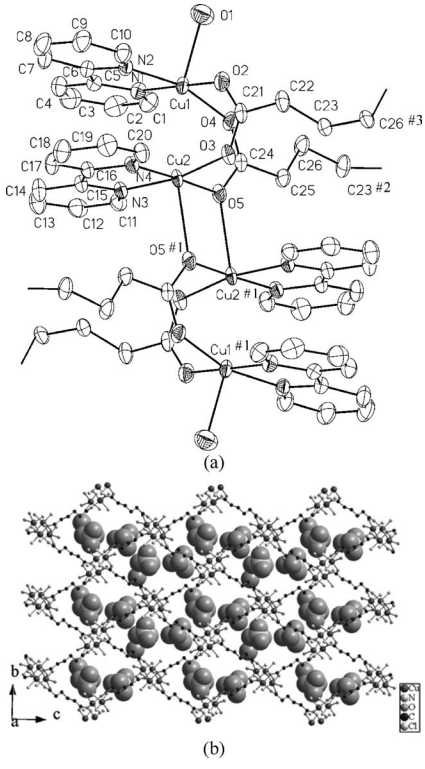

Figure 4. ORTEP view of the DSPW-like tetranuclear copper(II) clusters in **4** with atom numbering scheme and thermal ellipsoids drawn at 30% probability level (symmetry codes: #1 = $-x + 1, -y + 1, -z$; #2 = $-x + 1, y + 1/2, -z + 1/2$; #3 = $-x + 1, y - 1/2, -z + 1/2$); (b) crystal structure of **4** with perchlorate anions in space-filling mode (note that the coordinated bipyridine rings were omitted for clarity except the nitrogen atoms).

Thermal Analyses

Due to the highly explosive nature of perchlorate anions, thermal analysis was performed under a nitrogen atmosphere and the samples were handled carefully in small amounts. Thermogravimetric analysis of **3** (Figure S3) shows the polymer decomposes in three steps. The first weight loss of 2.2% in the range from 35 to 150 °C corresponds well to the removal of two coordinated water molecules (ca. 2.1%). An abrupt weight loss process with a sharp exothermic peak between 220 and 320 °C showed an explosive reaction between perchlorate anions and the organic ligands. However, the mass of residue less than 15.0% indicated a substantial loss of the copper element during the explosive stage. The TG-DTA curves of **4** displays similar thermal decomposition steps. The first weight loss of 4.5% between 35 and 150 °C corresponds to the calculated value (4.4%) for the removal of two coordinated water and two lattice water molecules, and the weight loss of 64.3% in the second step between 220 and 320 °C with a sharp exothermic peak could be attributed to the decomposition of four 2,2-bipyridine molecules, one and a half molecules of adipate ligands, and four perchlorate anions (ca. 65.2%). Upon further heating, the sample loses an additional weight of 8.7% over 340 to 500 °C in accordance with the removal of the remaining components (ca. 8.8%). The residue of 22.1% is assumed to be a mixture of CuO and CuCl (ca. 21.9%).

Magnetic Study

The magnetic susceptibility of powdered samples of compounds **3** and **4** were measured as a function of temperature 5–300 K in a fixed magnetic field 10000 Oe. The magnetic behaviors in the form of χ_m and $\chi_m T$ vs. T plots are depicted in Figure 5 (χ_m being the magnetic susceptibility for four Cu^{II} ions). For complex **3**, the value of χ_m at 300 K is 4.83×10^{-3} cm^3 mol^{-1}, which is less than the value of 4.99×10^{-3} cm^3 mol^{-1} for the spin-only value of four uncoupled Cu^{II} ions, indicating an orbital quenching.

Starting from room temperature, the χ_m value rises gradually to 0.010 cm^3 mol^{-1} at 79.9 K, and then falls sharply to 0.0036 cm^3 mol^{-1} at 24.0 K, revealing the occurrence of an overall antiferromagnetic coupling in **3**. The increase of the χ_m value at low temperature could be attributed to monomeric Cu^{II} impurities, as samples of **3** were separated manually from the deposit. Complex **4** behaves magnetically similar to **3**. The value of χ_m at 300 K is 4.34×10^{-3} cm^3 mol^{-1}. Upon cooling, the χ_m value rises gradually and go through a maximum (0.011 cm^3 mol^{-1}) at 75.1 K, and then falls to 1.06×10^{-4} cm^3 mol^{-1} at 15.0 K, indicating antiferromagnetic interactions. The paramag-

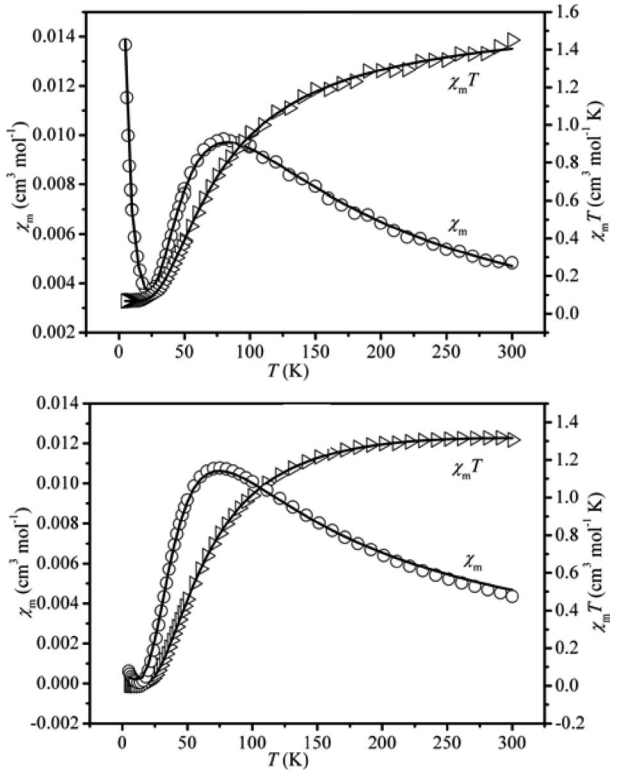

Figure 5. χ_m and $\chi_m T$ vs. T plots for complexes **3** (top) and **4** (bottom). The solid line represents the best theoretical fits.

netic tail of the χ_m value at low temperature could be attributed to the presence of a small amount of impurities.

It is worthy to point out that Ghosh et al. have recently analyzed the magnetic data of compound **4** in a dinuclear model; however, the magnetic data of Ghosh is to a certain extent confusing and the dinuclear mode is apparently too rough.[27] On one hand, the short distance between the Cu2 and Cu2$^{\#1}$ ions (3.378 Å) bridged by the two μ_2-O atoms in the apical–equatorial coordination mode indicates that the magnetic pathway, which is often operated by weak ferromagnetic interactions, can possibly not be neglected. One the other hand, the J value reported in the literature is surprisingly smaller than the J values of complexes with similar structural data just as described by the authors. Although they have tried to interpret the possible reasons of this reduction, it is still difficult to give a complete and accurate conclusion. Here we intend to fit the magnetic data of **3** and **4** in a linear tetranuclear Cu4 coupling system by taking into account the symmetry of the structure as well as the distances between the Cu^{II} ions (Scheme 2). Assuming $J_{12} = J_{1'2'}$, $J_{12'} = J_{1'2} = 0$, and $J_{11'} = 0$, the spin exchange Hamiltonian can be represented as $H = -2(2J_1S_1S_2 + J_2S_2S_{2'})$, where $J_1 = J_{12} = J_{1'2'}$, $J_2 = J_{22'}$. The expression of magnetic susceptibility is as follows:[28]

$$\chi_m = \frac{Ng^2\beta^2}{kT} \times \frac{x}{y} \times (1 - \rho) + \rho \times \frac{Ng^2\beta^2}{kT} + \text{TIP} \quad (1)$$

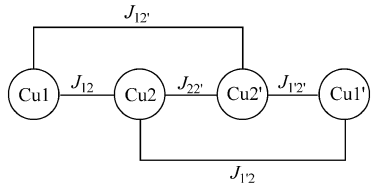

Scheme 2.

$x = 10\exp[-(-J_1 - 1/2J_2)/kT] + 2\exp[-(J_1 - 1/2J_2)/kT] + 2\exp\{-[1/2J_2 + (J_1^2 + J_2^2)^{1/2}]/kT\} + 2\exp\{-[1/2J_2 - (J_1^2 + J_2^2)^{1/2}]/kT\}$

$y = 5\exp[-(-J_1 - 1/2J_2)/kT] + 3\exp[-(J_1 - 1/2J_2)/kT] + 3\exp\{-[1/2J_2 + (J_1^2 + J_2^2)^{1/2}]/kT\} + 3\exp\{-[1/2J_2 - (J_1^2 + J_2^2)^{1/2}]/kT\} + \exp\{-[J_1 + 1/2J_2 + (4J_1^2 - 2J_1J_2 + J_2^2)^{1/2}]/kT\} + \exp\{-[J_1 + 1/2J_2 - (4J_1^2 - 2J_1J_2 + J_2^2)^{1/2}]/kT\}$

where N, g, and β are Avogadro's number, the g-factor, and the Bohr magneton, respectively, and k is Boltzman's constant. The parameter ρ denotes the fraction of paramagnetic impurity in the sample and a temperature independent paramagnetism (*TIP*) was also considered and fixed at 6.0×10^{-5} emu mol^{-1}. The experimental magnetic susceptibility data were fit to the theoretical expression in Equation (1), and the best fit was obtained with the following parameters: $g = 2.05$, $J_1 = -48.5$ cm^{-1}, $J_2 = 8.4$ cm^{-1} for complex **3** and $g = 2.03$, $J_1 = -41.6$ cm^{-1}, $J_2 = 8.7$ cm^{-1} for complex **4**. The relatively large negative J_1 value indicates that the *syn–syn* carboxylate bridges within the SPW unit mediate considerable antiferromagnetic coupling as expected, whereas the small positive J_2 value shows two μ_2-O(carboxylate) monoatomic bridges transmit a small ferromagnetic coupling consistent with the fact of a very small but not negligible coupling interaction through two Cu–O–Cu bridges within the Cu_2O_2 ring in apical–equatorial coordination mode.

Compared to the data of Ghosh, the magnetic data obtained in this work implies that the J value is more comparable with the complexes with similar structures and the consistency of the data of complexes **3** and **4** further ensure the rationality.

Electrochemistry

The redox behaviors of the complexes were studied by using cyclic voltammetry (CV). As shown in (Figure 6), the cyclic voltammogram of **3** exhibits two redox couples with the first oxidation peak at –0.230 V and the second at around 0.197 V. The corresponding reduction peaks were observed at –0.418 and –0.104 V. For complex **4**, two oxidation peak potentials at –0.232 and 0.225 V, as well as two reduction peak potentials at –0.458 and –0.085 V, were observed. The cyclic voltammograms of **3** and **4** are similar in their shapes and the shift of positions are also slight (0.02–0.04 V). These redox couples could be attributed to the process $Cu^{II}Cu^{II} \leftrightarrow Cu^{II}Cu^{I} \leftrightarrow Cu^{I}Cu^{I}$ by taking into account that there are two types of Cu^{II} ions in different coordination environments and no redox behavior of the organic ligands have been observed in the scanning range. The

i_{pc}/i_{pa} values for **3** and **4** suggest the processes are quasireversible and the positions of the peaks did not shift on repeated scanning.

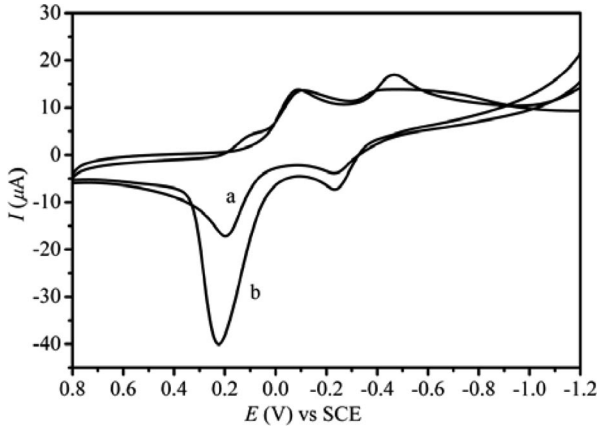

Figure 6. The cyclic voltammograms of complexes **3** (a) and **4** (b).

Conclusions

Self-assembly of Cu^{II} ions, adipate anions, and 2,2′-bipyridine/1,10-phenanthroline in aqueous methanolic solution yielded four adipato-bridged Cu^{II} complexes, $\{[Cu(phen)_2]_2(C_6H_8O_4)\}(ClO_4)_2$ (**1**), $\{[Cu(phen)_2]_2(C_6H_8O_4)\}(ClO_4)_2 \cdot 1.33H_2O$ (**2**), $[Cu_2(phen)_2(H_2O)]_2(C_6H_8O_4)_2(ClO_4)_4$ (**3**), and $\{[Cu_2(bpy)_2(H_2O)]_2(C_6H_8O_4)_2\}(ClO_4)_4 \cdot 2H_2O$ (**4**). The adipato-bridged dumbbell-like dinuclear $\{[Cu(phen)_2]_2(C_6H_8O_4)\}^{2+}$ complex cations in **1** and **2** proved to be good building blocks for the construction of (4,4)-type supramolecular networks. Utilization of the DSPW-like tetranuclear $\{[Cu_2(phen)_2(H_2O)]_2(COO)_4\}$ and $\{[Cu_2(bpy)_2(H_2O)]_2(COO)_4\}$ clusters in **3** and **4**, respectively, as SBUs provided an efficient strategy for the design and synthesis of more porous MOFs. Magnetic studies on the DSPW tetranuclear clusters of **3** and **4** indicate significant antiferromagnetic coupling interactions for the Cu^{II} ions bridged by the *syn–syn* carboxylate groups and weak ferromagnetic coupling for the copper(II) ions bridged by two μ_2-O atoms in the apical–equatorial coordination mode. Cyclic voltammograms of **3** and **4** exhibit similar behaviors, displaying two quasireversible redox couples in the range from –1.2 to 0.8 V. Exploitations of other DSPW-like tetranuclear metal clusters $\{[M_2L_2(H_2O)]_2(COO)_4\}$ as SBUs for the design and synthesis of novel MOFs are in progress.

Experimental Section

Reagents and Physical Measurements: All chemicals of reagent grade were commercially available and used without further purification. The infrared spectra were recorded from KBr pellets in the range 4000–400 cm^{-1} with an FTIR 8900 spectrometer. Single crystal data were collected with a Rigaku R-Axis Rapid IP X-ray diffractometer and a Bruker P4 diffractometer. The Powder X-ray diffractions were carried out with a Bruker D8 Focus X-ray diffractometer. Thermogravimetric measurement was performed under a flow of nitrogen gas from room temperature to 500 °C at a heating rate of 10 °C/min by using a Seiko Exstra 6000 TG/DTA 6300 apparatus and the temperature-dependent magnetic susceptibility was determined with a Quantum Design SQUID magnetometer (Quantum Design Model MPMS-7) in the temperature range 5–300 K. The cyclic voltammetric properties of **3** and **4** were studied in DMF solutions on a workstation from –1.2 to 0.8 V at a scan rate 0.1 $V s^{-1}$. The three-electrode system was composed of a glassy-carbon electrode as working electrode, an aqueous saturated calomel electrode as reference, and a platinum wire as counter electrode; tetrabutylammonium perchlorate was used as a supporting electrolyte. It was bubbled with nitrogen for several minutes prior to every measurement and all experiments were performed at room temperature.

$\{[Cu(phen)_2]_2(C_6H_8O_4)\}(ClO_4)_2$ (1) and $\{[Cu(phen)_2]_2(C_6H_8O_4)\}(ClO_4)_2 \cdot 1.33H_2O$ (2): $Cu(ClO_4)_2 \cdot 6H_2O$ (0.370 g, 1.0 mmol) was added to an aqueous methanolic solution of 1,10-phenanthroline monohydrate (0.198 g, 1.0 mmol) and adipic acid (0.146 g, 1.0 mmol) whilst stirring, and the mixture was adjusted to pH = 7.1 by dropwise addition of 1 M NaOH. After stirring for 30 min, the blue suspension was filtered, and evaporation of the pale-blue filtrate at room temperature yielded blue crystals of **1** and **2**. Much effort was dedicated to separate them from each other, unfortunately, all failed.

$[Cu_2(phen)_2(H_2O)]_2(C_6H_8O_4)_2\}(ClO_4)_4$ (3): 1,10-Phenanthroline monohydrate (0.198 g, 1.0 mmol) was added to a solution of adipic acid (0.073 g, 0.5 mmol) and $Cu(ClO_4)_2 \cdot 6H_2O$ (0.370 g, 1.0 mmol) in CH_3OH/H_2O (1:1, 40 mL). The mixture was adjusted to pH = 7.0 with 1 M NaOH. The blue suspension was stirred continuously for 30 min and then allowed to stand at room temperature. After several days, dark-blue block crystals were grown and could be readily separated from the deposit [yield: 30% based on the initial $Cu(ClO_4)_2 \cdot 6H_2O$ input]. The phase purity of the product was checked according to powder X-ray diffraction pattern compared with the simulated PXRD based on the single crystal data (Figure S1). IR (KBr): $\tilde{\nu}$ = 3442, 3087, 2937, 2866, 1566, 1519, 1430, 1398, 1087, 848, 719, 623 cm^{-1}.

$\{[Cu_2(bpy)_2(H_2O)]_2(C_6H_8O_4)_2\}(ClO_4)_4 \cdot 2H_2O$ (4): $Cu(ClO_4)_2 \cdot 6H_2O$ (0.370 g, 1.0 mmol) was added to a solution of 2,2-bpy (0.156 g, 1.0 mmol) and adipic acid (0.146 g, 1.0 mmol) in CH_3OH/H_2O (1:1, 40 mL) whilst stirring. Then the blue suspension was adjusted to pH = 7.2 with 1 M NaOH and stirred for 30 min. After filtration, the blue filtrate was allowed to stand at room temperature. Blue block crystals were grown by slow evaporation over several weeks. [yield: ca. 70% based on the initial $Cu(ClO_4)_2 \cdot 6H_2O$ input]. The product phase purity was checked according to powder X-ray diffraction pattern compared with the simulated PXRD based on the single crystal data (Figure S1). IR (KBr): $\tilde{\nu}$ = 3460, 3087, 2945, 2873, 1575, 1496, 1473, 1446, 1091, 623 cm^{-1}.

X-ray Crystallography: Suitable single crystals of **1**–**4** were selected under a polarizing microscope and fixed with epoxy cement on respective fine glass fibers. Compounds **1** and **2** were mounted on a Rigaku R-Axis Rapid IP X-ray diffractometer with graphite-monochromated Mo-K_α radiation (λ = 0.71073 Å) for cell determination and subsequent data collection, operating at 50 kV and 40 mA. The cell determination and subsequent data collection of **3** and **4** were performed with a Bruker P4 diffractometer with graphite-monochromated Mo-K_α Radiation, operating at 50 kV and 30 mA. Data was collected over the 2θ ranges 6–45° for **1**, 6–55° for **2**, and 3–55° for **3** and **4** at 295 K. All of the structures were solved by Patterson method and subsequent Fourier analyses and

Table 3. Summary of crystal data, data collection and structure refinement details for **1**–**4**.

	1	**2**	**3**	**4**
Empirical formula	$C_{54}H_{40}Cl_2Cu_2N_8O_{12}$	$C_{54}H_{42.67}Cl_2Cu_2N_8O_{13.33}$	$C_{60}H_{52}Cl_4Cu_4N_8O_{26}$	$C_{52}H_{56}Cl_4Cu_4N_8O_{28}$
Formula weight	1190.92	1214.94	1697.08	1637.03
Crystal system	monoclinic	monoclinic	triclinic	monoclinic
Space group	*C*2/*c*	*C*2/*c*	$P\bar{1}$	$P2_1/c$
a (Å)	21.522(4)	34.274(7)	10.1796(18)	15.032(3)
b (Å)	14.554(3)	13.787(3)	12.077(2)	11.726(2)
C (Å)	16.451(3)	32.424(7)	15.613(3)	18.443(4)
α (°)			67.474(11)	
β (°)	107.31(3)	94.78(3)	80.870(13)	95.47(3)
γ (°)			67.409(9)	
Volume (Å^3)	4919(2)	15269(5)	1636.8(5)	3236(1)
Z	4	12	1	2
$D_{calcd.}$ (g cm^{-3})	1.608	1.586	1.722	1.680
F(000)	2432	7456	860	1664
μ (mm^{-1})	1.050	1.018	1.509	1.553
θ Range (°)	3.09–22.50	3.02–27.48	1.41–27.50	1.36–27.51
Reflections collected	14366	73400	8589	9068
Unique reflections (R_{int})	3211	17400	7341	7424
Goodness of fit on F^2	1.046	1.009	1.031	1.036
R_1, wR_2 [$I \geq 2\sigma(I)$][a]	0.0709, 0.1834	0.0615, 0.1518	0.0524, 0.1526	0.0542, 0.1427
R_1, wR_2 (all data)[a]	0.1072, 0.2099	0.1326, 0.1829	0.0643, 0.1673	0.0795, 0.1603

[a] $R_1 = \Sigma(|F_o| - |F_c|)/\Sigma|F_o|$, $wR_2 = [\Sigma w(F_o^2 - F_c^2)^2/\Sigma w(F_o^2)^2]^{1/2}$, $w = [\sigma^2(F_o^2) + (aP)^2 + bP] - 1$, where $P = (F_o^2 + 2F_c^2)/3$.

refinement was performed by the full-matrix least-squares method based on F^2 with all observed reflections.[29,30] Hydrogen atoms of the organic groups were placed at their geometrically calculated positions, and those of water molecules were located on a difference Fourier map. The crystal data, intensity collection and details of structure refinement are summarized in Table 3.

CCDC-692098 (for **1**), -692099 (for **2**), -692100 (for **3**), -692101 (for **4**) contain the supplementary crystallographic data for this paper. These data can be obtained free of charge from The Cambridge Crystallographic Data Centre via www.ccdc.cam.ac.uk/data_request/cif.

Supporting Information (see footnote on the first page of this article): IR spectra, XRD powder diffraction patterns, and TG-DTA curves of **3** and **4**.

Acknowledgments

This project was sponsored by K. C. Wong Magna Fund in Ningbo University and supported by the Expert Project of Key Basic Research of the Ministry of Science and Technology of China (grant No. 2003CCA00800), the Zhejiang Provincial Natural Science Foundation (grant No. Z203067), and the Ningbo Municipal Natural Science Foundation (grant No. 2006A610061).

[1] J. M. Lehn, *Supramolecular Chemistry, Concepts and Perspectives*, VCH, New York, **1995**.
[2] L. Brunsveld, B. J. B. Folmer, E. W. Meijer, R. P. Sijbesma, *Chem. Rev.* **2001**, *101*, 4071–4097.
[3] N. C. Gianneschi, M. S. Masar, C. A. Mirkin, *Acc. Chem. Res.* **2005**, *38*, 825–837.
[4] E. Colacio, M. Ghazi, R. Kiveka1s, J. M. Moreno, *Inorg. Chem.* **2000**, *39*, 2882–2890.
[5] J. Yoon, E. I. Solomon, *Inorg. Chem.* **2005**, *44*, 8076–8086.
[6] Z. Ni, A. Yassar, T. Antoun, O. M. Yaghi, *J. Am. Chem. Soc.* **2005**, *127*, 12752–12753.
[7] E. Colacio, J.-P. Costes, R. Kivekas, J.-P. Laurent, J. Ruiz, *Inorg. Chem.* **1990**, *29*, 4240–4246.
[8] S. K. Dey, B. Bag, K. M. A. Malik, M. S. EI Fallah, J. Ribas, S. Mitra, *Inorg. Chem.* **2003**, *42*, 4029–4035.
[9] S. M.-F. Lo, S. S.-Y. Chui, L.-Y. Shek, Z. Lin, X. X. Zhang, G. Wen, I. D. Williams, *J. Am. Chem. Soc.* **2000**, *122*, 6263–6294.
[10] V. M. Rao, D. N. Sathyanarayana, H. Manohar, *J. Chem. Soc., Dalton Trans.* **1983**, 2167–2173.
[11] M. Eddaoudi, J. Kim, J. B. Wachter, H. K. Chae, M. O'Keeffe, O. M. Yaghi, *J. Am. Chem. Soc.* **2001**, *123*, 4368–4369.
[12] B. Moulton, J. J. Lu, M. J. Zaworotko, *J. Am. Chem. Soc.* **2001**, *123*, 9224–9225.
[13] S. S.-Y. Chui, S. M.-F. Lo, J. P. H. Charmant, A. G. Orpen, I. D. Williams, *Science* **1999**, *283*, 1148–1150.
[14] B. Chen, M. Eddaoudi, S. T. Hyde, M. O'Keeffe, O. M. Yaghi, *Science* **2001**, *291*, 1021–1023.
[15] H. Abourahma, G. J. Bodwell, J. J. Lu, B. Moulton, I. R. Pottie, R. B. Walsh, M. J. Zaworotko, *Cryst. Growth Des.* **2003**, *3*, 513–519.
[16] S. A. Bourne, J. J. Lu, A. Mondal, B. Moulton, M. J. Zaworotko, *Angew. Chem. Int. Ed.* **2001**, *40*, 2111–2113.
[17] B. Rather, M. J. Zaworotko, *Chem. Commun.* **2003**, 830–831.
[18] D.-H. Hu, W. Huang, S.-H. Gou, J.-L. Fang, H.-K. Fun, *Polyhedron* **2003**, *22*, 2661–2667.
[19] D. Ghoshal, T. K. Maji, G. Mostafa, S. Sain, T.-H. Lu, J. Ribas, E. Zangrando, N. R. Chaudhuri, *Dalton Trans.* **2004**, 1687–1695.
[20] L.-J. Zhou, X.-J. Luan, Y.-Y. Wang, G.-H. Lee, Q.-Z. Shi, S.-M. Peng, *J. Coord. Chem.* **2006**, *59*, 1107–1121.
[21] Y. F. Song, P. Gamez, A. F. Stassen, M. Lutz, A. L. Spek, J. Reedijk, *Eur. J. Inorg. Chem.* **2003**, 4073–4077.
[22] J. Foley, D. Kennefick, D. Phelan, S. Tyagi, B. Hathaway, *J. Chem. Soc., Dalton Trans.* **1983**, 2333–2338.
[23] G. Murphy, C. Murphy, B. Murphy, B. Hathaway, *J. Chem. Soc., Dalton Trans.* **1997**, 2653–2660.
[24] A. W. Addiso, N. Rao, *J. Chem. Soc., Dalton Trans.* **1984**, 1349–1356.
[25] Y.-Q. Zheng, J. Sun, J.-L. Lin, *Z. Anorg. Allg. Chem.* **2001**, *627*, 90–94.

[26] The structure of compound **2** could be found in CSD under the ref code RIFFAO, but the detailed structure description was not available.
[27] While this manuscript was in preparation, a report of this complex appeared: A. K. Ghosh, D. Ghoshal, E. Zangrando, J. Ribas, N. R. Chaudhuri, *Inorg. Chem.* **2007**, *46*, 3057–3071.
[28] S. R. Breeze, S. N. Wang, J. E. Greedan, N. P. Raju, *Inorg. Chem.* **1996**, *35*, 6944–6951.
[29] G. M. Sheldrick, *SHELXL-97: Program for Structure Determination*, University of Göttingen, Göttingen, Germany, **1997**.
[30] G. M. Sheldrick, *SHELXL-97: Program for Structure Refinement*, University of Göttingen, Göttingen, Germany, **1997**.
Received: March 27, 2008
Published Online: August 25, 2008

